Preparation of an Asymmetric Zeolite L Film

Mark C. Lovallo[1] and Michael Tsapatsis*

Department of Chemical Engineering
University of Massachusetts
Amherst, Massachusetts 01003

Tatsuya Okubo

Department of Chemical System Engineering
The University of Tokyo
7-3-1 Hongo, Bonkyo-ku, Tokyo 113, Japan

Received January 22, 1996
Revised Manuscript Received April 15, 1996

Zeolites and molecular sieves are widely used for catalysis and gas separations.[1] An elusive but highly rewarding goal is the fabrication of zeolite films for selective membranes,[2] electrodes,[3] sensors,[4] and optoelectronic devices.[5] Recently, a variety of techniques tailored to specific applications has emerged (postsynthesis preparations[6−9] as well as in situ film deposition[10−19]); however, to date, no general preparative methods exist.[20] Here we report on a new processing scheme which involves the use of zeolite nanosols (colloidal suspensions of zeolite nanoparticles) for film casting,[21] combined with controlled secondary growth of the nanoparticles. Decoupling film deposition from crystal growth provides added flexibility for tailoring the film microstructure and ease for scaleup. Implementation of this scheme, using zeolite L nanosols, led to the preparation of self-supported asymmetric zeolite L films. These films exhibit a regular decrease in crystal grain size and an increase in interzeolitic porosity proceeding from the intergrown surface of the film down into the bulk of the film. In this regard, we refer to these films as asymmetric, using the term as applied in membrane technology.[22]

Zeolite L Nanosols. The synthesis of zeolite L particles with crystal sizes as low as 20 nm has been reported in the literature by several researchers.[23−25] We have described the synthesis and characterization of zeolite L[26] nanoclusters in detail.[27,28] They consist of aligned zeolite crystalline domains of dimensions ∼40 nm in the channel direction and ∼15 nm in the direction perpendicular to the zeolite channels. The nanoclusters have an average size of 60 nm and possess inhomogeneities (intercrystalline porosity) on length scales ranging from 2 to 60 nm and a fractal dimension of ∼2.2 (estimated by small-angle X-ray scattering (SAXS)). Due to the small particle size and negative surface charge (the zeolite L nanocluster mobility was recorded as −3.64 μm/(s V cm) and the corresponding ζ-potential −46.7 mV, at pH∼7) stable zeolite L suspensions (nanosols) in water (pH ∼ 7) can be prepared with concentrations up to 35 g (zeolite L)/L.

Film Casting from Zeolite Nanosols. The zeolite L nanosols were used for the preparation of unsupported films.[27] Supported films can also be prepared, by spin-coating or dip-coating, with almost no limitations imposed upon the choice of substrate, in contrast to in situ preparations. The pure zeolite films are microcrack free and translucent. The ability to utilize suspensions of zeolite crystals for film preparation through colloidal suspension processing renders this technique a powerful tool for efficient film production. A thick (2 mm) unsupported film is shown in Figure 1a along with a field emission scanning electron microscopy (FE-SEM) top view (Figure 1b).

The films are fragile since the zeolite clusters are not chemically bonded via strong chemical bonds. The addition of a binder can enhance the mechanical strength and integrity of the films. For the preparation of a zeolite L−Al_2O_3 film the addition of a boehmite[29] sol to a zeolite L nanosol was followed by stirring. Upon mixing agglomeration was observed caused by the opposite surface charges of zeolite and alumina particles (the ζ potential for the alumina suspension in water is ∼40 mV while for the zeolite suspension it is ∼−46.7 mV). The dispersion was used for film casting, resulting in a composite, opaque film with increased mechanical strength. Nitrogen adsorption isotherms reveal a small decrease in interzeolitic porosity for composite zeolite/alumina films as compared to pure zeolite films but no change in the microporosity, indicating no blockage of

* Corresponding author.

(1) Davis, M. E. *Ind. Eng. Chem. Res.* **1991**, *30*, 1675 and references therein.
(2) Hennepe, H. J. C.; Bargeman D.; Mulder M. H. V.; Smoulders, C. A. *J. Membr. Sci.* **1987**, *35*, 39.
(3) Rolison D. R. *Chem. Rev.* **1990**, *90*, 867.
(4) Ozin G. A.; Kuperman, A.; Stein, A. *Angew. Chem., Int. Ed. Engl.* **1989**, *28*, 359.
(5) Werner, L.; Caro, J.; Finger, G.; Kornatowski, J. *Zeolites* **1992**, *12*, 658.
(6) Bein, T.; Brown, K.; Brinker, C. J. *Zeolites: Facts, Figures, Future*; Elsevier Science Publishers B. V.: Amsterdam, 1989.
(7) Hennepe, H. J. C.; Mulder, M. H. V.; Smolders, C. A.; Bargeman, D.; Schroeder, G.A. T. *Pervaporation process and membrane*, US Patent 4,925,562, 1990.
(8) Jia, M.; Peinmann, K. L.; Behling, R. D. *J. Membr. Sci.* **1991**, *57*, 289.
(9) Bein, T.; Brown, K. *J. Am. Chem. Soc.* **1989**, *111*, 7641.
(10) Anderson, M. W.; Pachis, K. S.; Shi, J.; Carr, S. W. *J. Mater. Chem.* **1992**, *2*, 255.
(11) Sano, T.; Kiyozumi, Y.; Kawamura, M.; Mizukami, F.; Takaya, H.; Mouri, T.; Inaoka, W.; Toida, Y.; Watanabe, M.; Toyoda, K. *Zeolites* **1991**, *11*, 842.
(12) Yan Y.; Tsapatsis, M.; Gavalas, G. R.; Davis, M. E. *J. Chem. Soc., Chem. Commun.* **1995**, *227*.
(13) Geus, E. R.; van Bekkum, H.; Bakker, W. J. W.; Moulijn, J. A. *Microporous Mater.* **1993**, *1*, 131.
(14) Jia, M. D.; Chem, B.; Noble, R. D.; Falconer, J. L. *J. Membr. Sci.* **1994**, *90*, 1.
(15) Yamazaki, S.; Tsutsumi, K. *Microporous Mater.* **1995**, *4*, 205.
(16) Sano, T.; Hasegawa, M.; Kawakami, Y.; Kiyozumi, Y.; Yanagishita, H.; Kitamoto, D.; Mizukami, F. *Stud. Surf. Sci. Catal.* **1994**, *85*, 1175.
(17) Sano, T.; Ejiri, S.; Hasegawa, M.; Kawakami, Y.; Enomoto, N.; Tamai, Y.; Yanagishita, H. *Chem. Lett.* **1995**, *2*, 153.
(18) Yan, Y.; Davis, M. E.; Gavalas, G. R. *Ind. Eng. Chem. Res.* **1995**, *34*, 1652.
(19) Tsikoyainnis, J. G.; Haag, W. O. *Zeolites* **1992**, *12*, 126.
(20) Armor, J. *Chem. Mater.* **1994**, *6*, 730.
(21) Tsapatsis, M.; Okubo, T.; Lovallo, M.; Davis, M. E. *Mater. Res. Soc. Symp. Proc.* **1995**, *371*, 21.
(22) Bhave, R. R. *Inorganic Membranes: Synthesis, Characteristics, and Applications;* Van Nostrand Reinhold: New York, 1991.
(23) Verduijn, P. V.; Mechilium, J.; De Gruijter, C. B.; Koetsier, W. T.; Van Oorschot, C. W. M. U.S. Patent 5,064,630, 1991.
(24) Meng, X.; Zhang, Y.; Meng, C.; Pang, W. In *Proceedings of the 9th International Zeolite Conference;* von Ballmoos, R., et al., Eds.; Butterworth-Heinemann: Boston, 1993.
(25) Vaughan, D. E. W.; Strohmaier, K. G. Canadian Patent Application, 1994.
(26) Meier, W. M.; Olson, D. H. *Atlas of Zeolite Structure Types*, 3rd ed.; Butterworth-Heinemann: London, 1992.
(27) Tsapatsis, M.; Lovallo, M.; Okubo, T.; Davis, M. E; Sadakata, M. *Chem. Mater.* **1995**, *7*, 1734.
(28) Tsapatsis, M.; Lovallo, M.; Davis, M. E *Microporous Mater.* **1996**, *5*, 381.
(29) Lao, H.; Detellier, C.; Matsuura, T.; Tremblay, A. Y. *J. Mater. Sci. Lett.* **1994**, *13*, 895.

S0897-4756(96)00037-3 CCC: $12.00

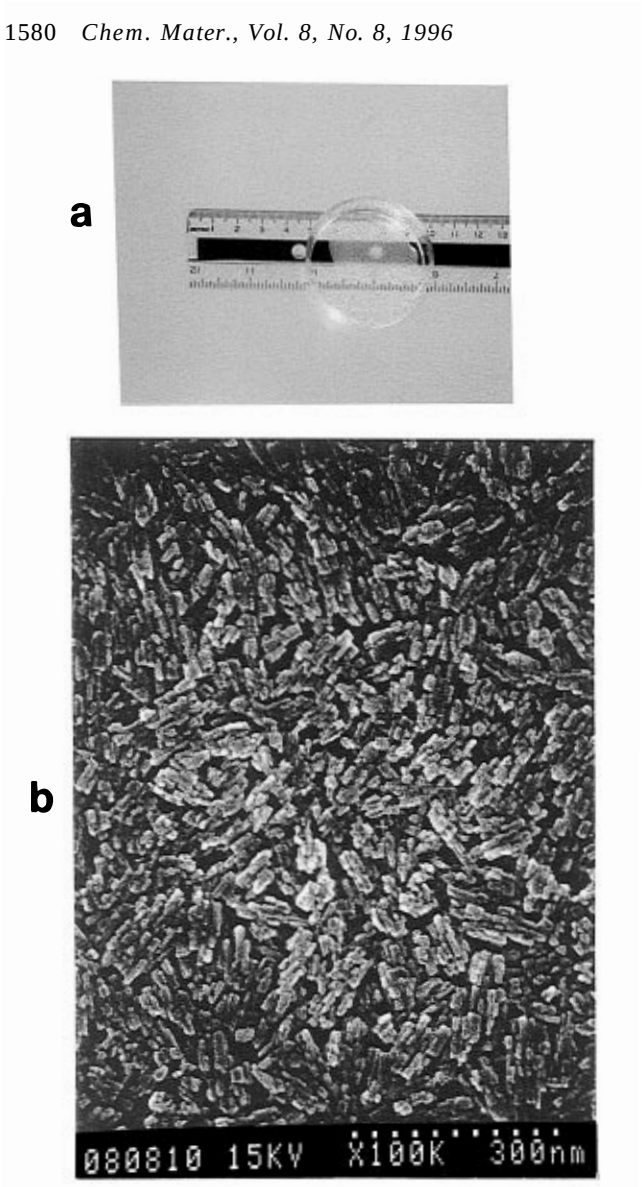

Figure 1. (a) Thick self-supported zeolite L film prepared by slow evaporation of the water from a zeolite L nanosol placed in a petri dish. The surface of the petri dish was treated with wax in order to be rendered hydrophobic and avoid film cracking. (b) Top view field emission scanning electron microscopy (FE-SEM) image of the film shown in Figure 1a. Microscope operating conditions and sample preparation were as described in ref 22. (c) Pore size distribution from nitrogen adsorption of zeolite film compared to zeolite/alumina film.

the zeolite pores. The pore size distribution is given in Figure 1c.

The pores between the zeolite particles (interzeolitic porosity) have sizes of the order of the zeolite particle size (<100 nm) as suggested by nitrogen adsorption and FE-SEM. However, for molecular sieving applications the interzeolitic porosity should be eliminated. To achieve this elimination, conditions were identified under which zeolite nanoclusters grow to larger, more compact particles without the nucleation of new crystallites.[27] We refer to this seeded process as secondary growth.

Secondary Growth. The regrowth experiment relevant to this communication is described below: Aluminum foil (2.0 mm thick, 99.99 ± %, Aldrich) and fumed silica (Grade M-5, Cabosil) were used to prepare aluminate solutions and silicate solutions, respectively. The alkali-metal ion source was potassium hydroxide (ACS grade, Fisher). A 10 g/L zeolite suspension (10 mL) in water was added to 30 mL of a homogeneous solution with composition $10K_2O-1Al_2O_3-25SiO_2-900H_2O$, resulting in a solution with composition $10K_2O-1Al_2O_3-25SiO_2-1200H_2O$−54 g of nanocluster seeds. Reactants were placed in Teflon-lined stainless steel vessels and heated at 150 °C for 6 h. In a control experiment, a solution with composition $10K_2O-1Al_2O_3-25SiO_2-1200H_2O$ with no added seeds was subjected to the same heating procedure. In the absence of zeolite L seed crystals, we observe the formation of an amorphous gel followed by the precipitation of an amorphous phase. In the presence of nanoclusters the amorphous gel formed encapsulates the zeolite nanoclusters and is gradually consumed for further crystal growth, and no amorphous precipitate remains at the end of secondary growth. Additional crystal yield after regrowth corresponds to approximately 100% consumption of the available aluminum for regrowth (zeolite L grows at a specific Si/Al ratio of 3[27]). Figure 2b shows a transmission electron microscope (TEM) image of the regrown crystals. The morphology of the crystals before regrowth is shown in Figure 2a. Micrographs were recorded using the JEOL ARM-1000 operating at 800 kV at The National Center for Electron Microscopy. For transmission electron microscopy a drop of the zeolite suspension in water was transferred to a carbon-coated Cu grid. The grid was allowed to dry at 110 °C and was mounted on a single-tilt liquid nitrogen cooled specimen holder.

Asymmetric Film Formation. The regrowth conditions identified in the experiment described above were implemented in order to eliminate the interzeolitic porosity of the cast zeolite/alumina films: film sections (93% zeolite/7% alumina, 5 mm × 5 mm × 0.3 mm, calcined at 725 °C for 2 h) were held vertically in contact with 30ml of a homogeneous solution of composition $10K_2O-1Al_2O_3-25SiO_2-1200H_2O$ and heated in Teflon-lined stainless steel vessels at 150 °C for up to 6 h. Films removed at various times were washed in distilled water, dried, and calcined to 750 °C. The FE-SEM top views of a series of films obtained by this procedure are shown in Figure 3 (for the films shown in Figure 3b,c the calcination step was omitted). After 3 h of regrowth a small increase of the nanocrystal's size is observed while the presence of gel between crystallites is evident. After 6 h a drastic change of the film morphology takes place. Figure 3c (uncalcined) and d (calcined at 700 °C for 2 h) reveal larger cylindrical crystals closely packed

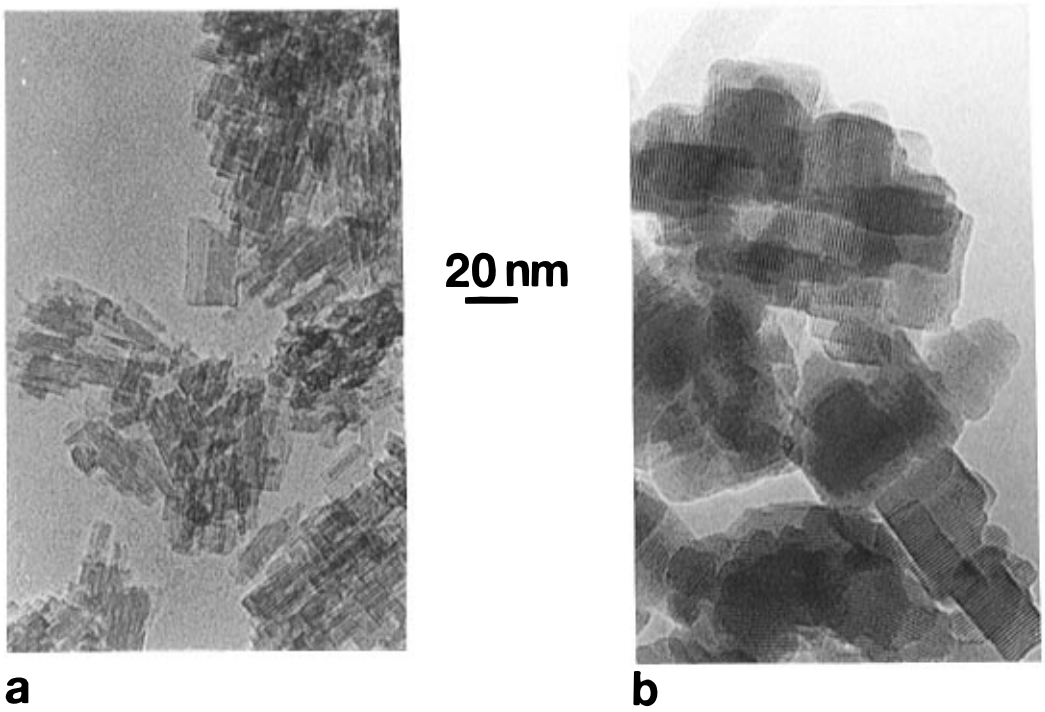

Figure 2. (a) Transmission electron microscopy (TEM) image of zeolite L (structure code LTL) nanoclusters. Sample preparation, image acquisition and synthesis conditions as in ref 22. (b) TEM image of regrown crystals.

and intergrown and a surface with reduced interzeolitic porosity (no interzeolitic porosity to the resolution of the FE-SEM). Small fragments of unconverted gel are occasionally observed on the surface emanating for the zeolite crystals (Figure 3c). The cylindrical morphology of crystals is common to zeolite L. TEM (described below) confirms that the crystals present on the surface are zeolite L.

Further analysis was performed by TEM. Figure 4a is a low-resolution TEM image of a microtomed cross section of the film presented in Figure 3c,d. Sample preparation was done by microtomy: after embedding in epoxy, the films were microtomed using a Diatome diamond knife. Figure 4a shows a gradual decrease in crystal size and an increase in interzeolitic porosity across the thickness of the film. The largest crystals at the top of the film (area A) are followed by crystals with decreasing grain size (area B) and eventually by nanocrystals which experienced little if any regrowth (area C where the interzeolitic porosity is not altered). As the grain size decreases, the interzeolitic porosity increases. Also apparent in Figure 4a are "wormlike" cracks that run from the top of the film to the interior of the film (from area A to C). The cracks are a few hundred angstroms wide and a few hundred angstroms apart. These cracks are typical of microtomed samples and are not features of the film. During microtomy, as the diamond knife edge cuts the sample, the sample is compressed and deformed. Soft or polycrystalline materials (as in this case) tend to undergo slip on a fine scale under the stress of the knife.[30] This causes cracks or inhomogeneities parallel to the knife edge (as seen in Figure 4a). The crack size and crack repeat distance are smaller than the crystal grain size at the film surface. If these cracks were a feature of the film, they would be apparent in the FE-SEM views of Figure 3. Therefore, the cracks seen in this figure were introduced during sample preparation. Disregarding these cracks, area A exhibits no interzeolitic porosity (to the resolution of the FE-SEM and TEM) and constitutes a thin (~200 nm), intergrown, and continuous layer. In area C, interzeolitic porosity is on the order of the zeolite particle size (~100 nm).

Both HREM and electron microdiffraction[31] (not shown) fail to reveal the presence of alumina in the as-cast and regrown films. This observation suggests that the alumina is finely divided and most probably has coated the external surfaces of the zeolite particles. This behavior can be attributed to the opposing charges of the alumina and zeolite particles in water (pH ~ 7).

The HREM images of Figure 4b,c indicate that crystal orientation is random with crystallites oriented with their *c* axis from nearly perpendicular to the film plane (Figure 4b) to parallel to the film plane (Figure 4c). The cylindrical morphology of the crystals at the top layer is in agreement with the FE-SEM top view (Figure 3c,d).

Since no crystalline products are formed in the absence of seed crystals, it is suggested that the continuous top layer of intergrown crystals evolves from the secondary growth of the zeolite nanoclusters at the surface of the film. The interplay between crystal growth and transport of precursor species account for the asymmetric morphology of the regrown film. Nanoclusters toward the center of the film receive a limited amount of nutrients, while crystals near the surface have an abundant supply of reacting species. Moreover, the zeolite L secondary growth proceeds through a precursor gel phase which upon its formation further contributes to the final asymmetric film microstructure by limiting the transport of nutrients to the interior of

(30) Hirsch, P.; Howie, A.; Nicholson, R.; Pashley, D. W.; Whelan, M. J. *Electron Microscopy of Thin Crystals*, 2nd ed.; Robert E. Kreiger Publishing Co.: FL, 1977.

(31) Spence, J. C. H.; Zuo, J. M. *Electron microdiffraction*; Plenum Press: New York, 1992.

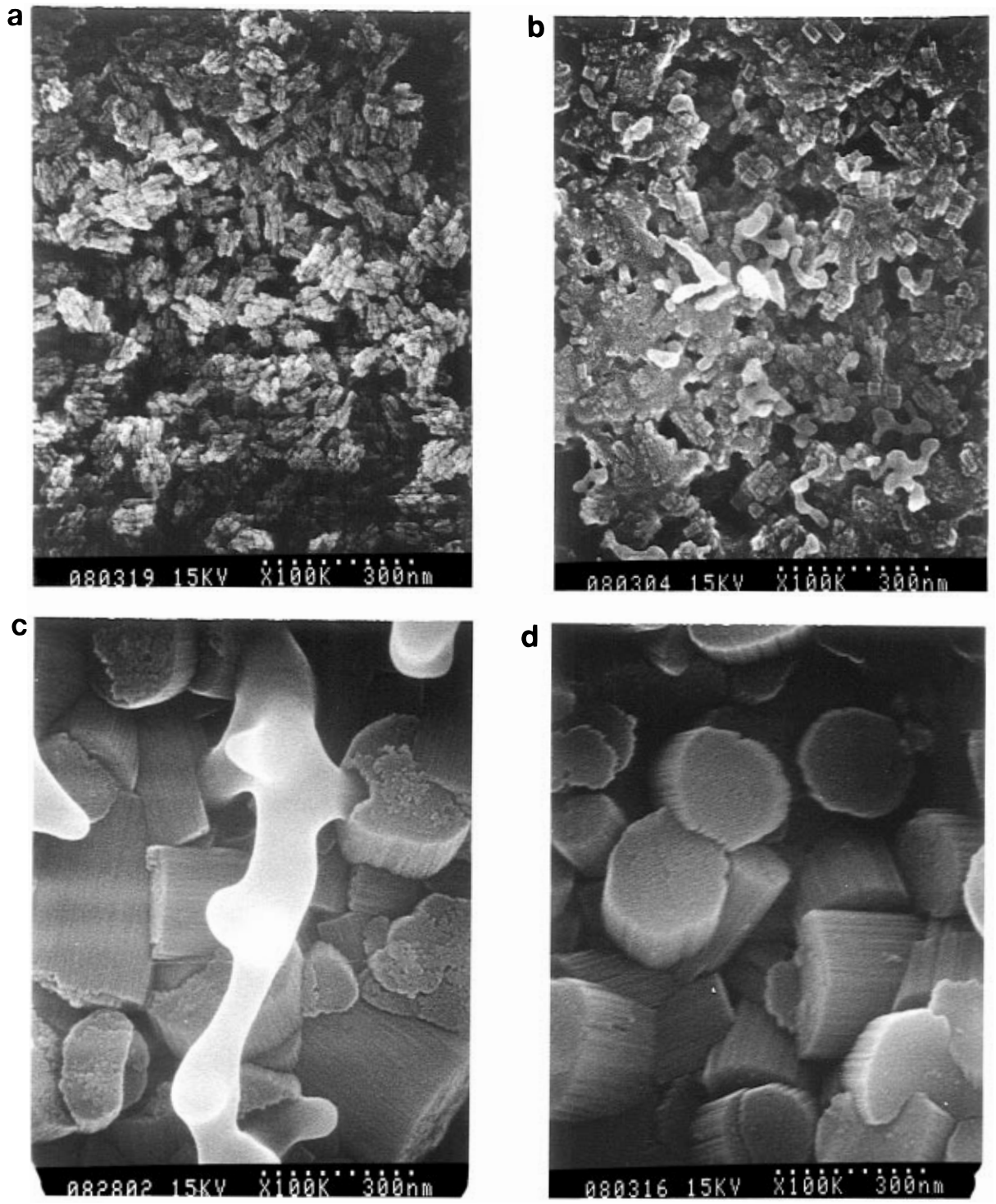

Figure 3. FE-SEM top views of (a) calcined zeolite/alumina film; (b) film in Figure 3a after 3 h of secondary growth; (c) (uncalcined) and (d) (calcined): film in Figure 3a after 6 h of secondary growth.

the film. The presence of small fragments of unconverted gel connecting the exposed faces of the crystals (Figure 3c) further corroborates the proposed mechanism. The use of nanocrystalline zeolites for the precursor film preparation is crucial for fabricating more dense films with reduced interzeolitic porosity. This makes it possible for the zeolite particles to intergrow during the secondary growth process.

To our knowledge this is the first report of the formation of a thin intergrown zeolite layer through the secondary growth of a prefabricated zeolite film. Current work is directed toward the expansion of this technique to thin supported films and utilization of other zeolite suspensions (zeolites A and Y,[32] silicalite,[33] ZSM-5[34,35]).

(32) Otterstedt, J. E.; Sterte, J. *Micro Particles*, International Patent WO 94/05597, 1993.
(33) Persson, A. E.; Schoeman, B. J.; Sterte, J.; Otterstedt, J. E. *Zeolites* **1994**, *14*, 557.
(34) Yamamura, M.; Chake, K.; Wakatsuki, T.; Okado, H.; Fujimoto, K. *Zeolites* **1994**, *14*, 643.
(35) Persson, A. E.; Schoeman, B. J.; Sterte, J.; Otterstedt, J. E. *Zeolites* **1995**, *15*, 611.

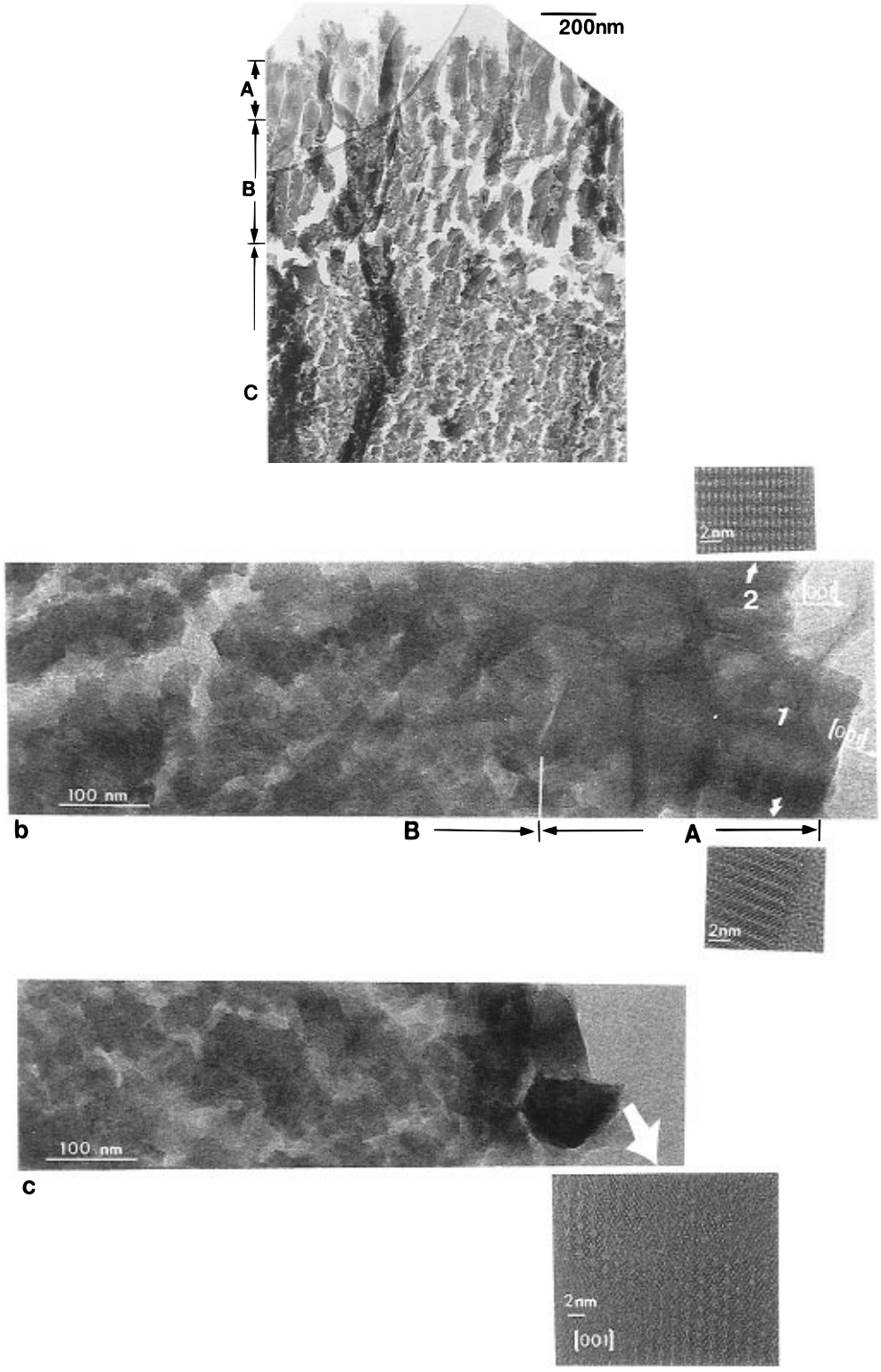

Figure 4. TEM cross sections of regrown film shown in Figure 3c,d. (a) Low magnification of cross section showing asymmetric feature of regrown film. Crystal grain size decreases from top intergrown layer (A) through intermediate sized grains (B) to innermost nanocrystals (C). (b) High magnification of cross section. Grain boundary can be seen between crystals 1 and 2 in top intergrown layer. The c-directions of crystals 1 and 2 are indicated in the figure. High-resolution micrographs (HREM) are consistent with zeolite L (insets). (c) High magnification of cross section. Crystal with view down the *c* axis can be seen in top intergrown layer. High-resolution micrograph (HREM) is shown at the inset.

Acknowledgment is made to the donors of the Petroleum Research Fund, Administered by the American Chemical Society, for support of this research. M.T. is grateful to the National Center for Electron Microscopy/ Department of Energy for a NCEM/DOE visiting fellowship. The assistance of C. Echer, C. Nelson at NCEM, Professor S. Suib (for providing access to XRD facility), Professor W. C. Conner (for the nitrogen adsorption), and Professor Mark E. Davis (for suggestions) is greatly appreciated. Finally, we acknowledge the W. M. Keck Polymer Morphology Laboratory for use of its Electron Microscopy Facilities.

CM960037B